J. Fluid Mech. (1977), *vol.* 83, *part* 2, *pp.* 311–335
Printed in Great Britain

Heat transport and thermal structure in the interfacial boundary layer measured in an open tank of water in turbulent free convection

By KRISTINA B. KATSAROS, W. TIMOTHY LIU, JOOST A. BUSINGER AND JAMES E. TILLMAN

Department of Atmospheric Sciences, University of Washington, Seattle

(Received 20 May 1976)

The thermal structure in the boundary layer and its relation to the heat flux from the cooling and evaporating surface of a deep tank of water are investigated. When a deep layer of water in contact with still air above loses heat to the air, the cooled water in a region just under the surface converges along lines and then plunges down in sheets. These sheets of falling water dissipate as they move into the body of the water, which is in turbulent motion. The vertical profiles of the horizontally averaged temperature and its standard deviation agree fairly closely with theoretical profiles based on time averages of the solution to the heat diffusion equation. The differences between observed and thus predicted profile shapes are consistent with the expected effects of the falling cold thermals and the warm return flow, which are neglected in the theories. The profiles of the standard deviation have large values up to the interface and lie between predictions based on boundary conditions of constant surface temperature and constant heat flux, in keeping with the experimental conditions.

The relation between the net heat flux and the temperature difference across the boundary layer is given in non-dimensional form by

$$N = 0{\cdot}156R^{0{\cdot}33},$$

which is in good agreement with the asymptotic similarity prediction $N \propto R^{\frac{1}{3}}$ but lower than theoretical calculations of the upper bound of N *vs.* R.

1. Introduction

The body of a deep layer of water in convection is rather well mixed and the temperature is nearly constant. Next to the boundary, however, motions are constricted, and there exists a boundary layer where molecular transport dominates. It is within this boundary layer that most of the temperature gradient in the fluid occurs.

The existence of a cool boundary layer on the surface of natural water bodies due to net upward heat flux has long been known (e.g. Woodcock 1941; Woodcock & Stommel 1947; Ball 1954; Ewing & McAlister 1960; Hasse 1963; Katsaros 1973; see Roll 1965 for a summary of earlier studies). The temperature drop across the boundary layer introduces a significant difference between the bulk water temperature and the temperature obtained by remote sensing devices, which receive radiation from the top 10–50 μm. It is often important to know this difference.

In a series of papers (McAlister 1964, 1967, 1969; McAlister & McLeish 1969, 1970; McAlister, McLeish & Corduan 1971) a technique was developed for measuring the total heat flux from the sea remotely by analysing the output of a two-wavelength radiometer which effectively measured the temperature at two optical depths in the water because of the dependence of the absorption coefficient on wavelength. By assuming that the temperature gradient was linear over the depth difference, the heat flux could be deduced. This technique was successful in obtaining agreement with climatological and other heat flux data to within 10–20 %. This established some faith in a conduction region. The average temperature profile can, however, furthermore be shown to be nonlinear when convergence and divergence are present (Katsaros & Businger 1973) or when the boundary layer is unsteady owing to buoyancy forces or shear stresses. It will be shown by photographs that such 'surface renewal' occurs very close to the interface. How close to the interface the significant deviations from linearity occur is, of course, important for the use of the two-wavelength radiometer technique.

Previous experimental studies have mainly been performed on the thermal convection between parallel plates uniformly heated from below and cooled from above (e.g. R. J. Schmidt & Saunders 1938; G. Schmidt & Silveston 1959; Globe & Dropkin 1959; Malkus 1954*a*; Rossby 1969; Chu & Goldstein 1973; Goldstein & Chu 1969; Deardorff & Willis 1967*a*, *b*; Willis & Deardorff 1967*a*, *b*; Carrol 1971; Fitzjarrald 1976). Convection below a free surface of deep water has not been adequately studied, even though it is such a common geophysical phenomenon; exceptions are studies by Ramdas & Raman (1946), Häussler (1956), Spangenberg & Rowland (1961) and Foster (1965). Berg, Acrivos & Boudart (1966) studied convection in evaporating shallow liquids and discussed effects of surface tension, surfactants and the depth of the fluid.

In many of these experimental studies the mean temperature profiles within the bulk of the medium and the horizontal length scales were obtained (e.g. Deardorff & Willis 1967*a*, *b*; Carrol 1971; Fitzjarrald 1976). Owing to the limited size of our facility, we have concentrated on making measurements within the thermal boundary layer below a free water surface. The measured thermal structure is compared with the theoretical predictions of the mean temperature profile by Howard (1966) based on boundary-layer instability and with a generalization of this theory by Liu & Businger (1975).

Classical experimental and theoretical studies of free convection have determined the functional relationship between the two non-dimensional quantities: the Nusselt number, a measure of the heat flux, and the Rayleigh number, a stability parameter. This relationship is also examined for the case of a deep water tank with heat flux across one free boundary.

2. Historical background

Bénard (1901) was the first to demonstrate in a definitive manner the onset of convection in a fluid. The gravitational stability problem of a cooled fluid was subsequently studied by Rayleigh (1916) and extended by Jeffreys (1926, 1928), Low (1929), Pellew & Southwell (1940) and others to various boundary conditions. The linear theory of thermal convection is summarized by Chandrasekhar (1961).

At a free surface, instability can also be induced by surface-tension variations. Through a theoretical approach parallel to those used in the studies of instability due

to buoyancy, the marginal stability criterion was found by Pearson (1958) to be given by a critical Marangoni number.† For a critical Rayleigh number of 571 and a critical Marangoni number of 80, he determined, however, that in water depths greater than 10 mm buoyancy forces are more effective than surface-tension forces in producing instability.

Townsend (1959) and Sparrow, Husar & Goldstein (1970) studied the formation of thermals in air and water respectively. Three studies on the thermal structure below a free water surface in 6–10 cm deep vessels have been reported (Ramdas & Raman 1946; Häussler 1956; Spangenberg & Rowland 1961). For a moderately large upward heat flux a water body of this depth will be characterized by a Rayleigh number $\simeq 10^5$–10^6. At these Rayleigh numbers the convection begins to be turbulent (Willis & Deardorff 1965, 1967*a*; Krishnamurti 1970, 1973). Ramdas & Raman, Häussler and Spangenberg & Rowland measured the temperature profiles through the air–water interface for varying conditions of sensible and latent heat flux using thermoelectric sensors. Under conditions of upward heat flux all three studies show a layer below the interface a few millimetres thick where the temperature gradient increases rapidly towards the interface. Spangenberg & Rowland say of the temperature deviation from the bulk temperature that 'this temperature difference varies approximately exponentially with depth'. These authors also found, using schlieren photography, that the cool water on the surface collects along lines, producing thickened regions of the boundary layer. When these regions become unstable, the cool water plunges down in vertical sheets, reducing the thickness of the surface layer. The horizontal pattern of convection lines is irregular and changes with time.

Willis & Deardorff (1967*a*) and Rossby (1969) investigated the spectral characteristics of time series of temperature obtained away from the boundary layers in air, water and Dow Corning 200 Fluid. They found short period peaks in the spectra and attributed the origin of these fluctuations to boundary-layer instabilities. Numerical studies by Elder (1969) and Foster (1971) also indicated cyclic instability of the boundary layer. Such instabilities were also described by Higbie (1935) and Danckwerts (1951), who proposed the so-called 'penetration' and 'surface renewal' models for gas absorption by a turbulent liquid. A mass-transfer coefficient was derived by using the diffusion equation coupled with a distribution function for the contact time of fluid elements near the interface. Howard (1966) derived an average temperature profile and the maximum standard deviation in the sublayer in terms of the period of the conductive phase. Liu & Businger (1975) generalized these models and derived flux-profile relations for both free and forced convection under two different boundary conditions.

When instability is caused only by an adverse temperature gradient and the fluid elements at the surface take equal times to reach instability, the flux-profile relations are

$$(\overline{T} - T_b)/(\overline{T}_s - T_b) = 4i^2 \operatorname{erfc}[\pi^{\frac{1}{2}} z/4\delta] \tag{1}$$

for constant boundary temperature and

$$(\overline{T} - T_b)/(\overline{T}_s - T_b) = \pi^{\frac{1}{2}} 6i^3 \operatorname{erfc}[2z/3\pi^{\frac{1}{2}}\delta] \tag{2}$$

† $M = -\dfrac{\partial\gamma}{\partial T}\dfrac{\partial T}{\partial z} d^2(\rho\nu\kappa)^{-1}$, where γ is the surface tension, d the fluid depth, ρ the density, ν the kinematic viscosity and κ the thermal diffusivity $k/\rho c_p$.

for constant heat flux through the boundary where, T_b is the bulk temperature, T_s is the surface temperature and an overbar denotes a temporal or horizontal average. When the time for fluid elements at the surface to reach instability is randomly distributed, the flux-profile relation for both boundary conditions is

$$(\bar{T} - T_b)/(\bar{T}_s - T_b) = \exp(-z/\delta). \tag{3}$$

Under the assumption of instantaneous boundary-layer collapse an observed temperature profile within the boundary layer is expected to lie between these two extremes. In these relations, δ is a scaling length defined by

$$\delta = -k(\bar{T}_s - \bar{T}_b)/\bar{Q}, \tag{4}$$

where Q is the heat flux. One aim of this study is to look further into the formation of plumes under a cooling water surface by visualization of the flow in the boundary layer and by measuring the mean temperature distribution and the characteristics of the fluctuations there.

Numerous experimental studies on convection between rigid boundaries have been devoted to finding the relationship between the Nusselt, Rayleigh and Prandtl numbers, since such an interdependence can be predicted by dimensional reasoning (e.g. Mull & Reiher 1930; R. J. Schmidt & Milverton 1935; Malkus 1954*a*; G. Schmidt & Silveston 1959; Globe & Dropkin 1959; Willis & Deardoff 1967*b*; Rossby 1969; Somerscales & Gazda 1969; Goldstein & Chu 1969; Chu & Goldstein 1973).

The dependence of the Nusselt number on the Prandtl number was found to be weak (e.g. Globe & Dropkin 1959; Willis & Deardorff 1967*b*; Krishnamurti 1970, 1973) and the studies concentrated on finding the constants A_* and n in the relationship

$$N_* = A_* R_*^n, \tag{5}$$

where N_* and R_* are the Nusselt and Rayleigh numbers for a fluid with two boundary layers. The value of n ranges from 0·25 to 0·50 and that of A_* from 0·06 to 0·76. However, the exponent was found to exhibit discrete changes with increasing Rayleigh number, which were associated with transitions from one mode of convection to another (see Krishnamurti 1973).

Malkus (1954*b*) derived a relationship between N_* and R_* based on the hypothesis that the flow seeks to maximize the heat transport. This idea was generalized by Howard (1963), who used the variational method to determine the upper bound on the heat flux under the constraint of a set of 'power integrals' which are integral relations expressing the balance of energy and entropy. He found $N_* \leqslant (\frac{3}{64}R_*)^{\frac{1}{2}}$. Under the additional constraints of continuity and a single horizontal wavenumber, he found $N_* \leqslant (\frac{1}{2\,4\,8}R_*)^{\frac{1}{3}}$. Busse (1969) extended the variational method to allow multiple boundary-layer structure, and found the upper bound to be $N_* \leqslant (\frac{1}{1\,0\,3\,5}R_*)^{\frac{1}{2}}$ for large R_*.

Numerical methods have also been used to study the $N_* vs. R_*$ relation (Herring 1963, 1964; Foster 1971; Straus 1973, 1976). Herring selected the wavenumber which maximized the flow and found $N_* = 0{\cdot}31R_*^{\frac{1}{2}}$ for two free boundaries and $N_* = 0{\cdot}135N_*^{\frac{1}{3}}$ for two rigid boundaries. Thus there is an increase in the coefficient with free rather than rigid boundaries. Straus (1973) compares upper-bound calculations of the Nusselt number for convection between two rigid and two free boundaries respectively. He finds convection between two free boundaries to be twice as effective, but the power

remains constant. Moore & Weiss (1973) found a power greater than $\frac{1}{3}$ for water convection between free boundaries at Rayleigh numbers up to $O(10^7)$ for cell widths equal to the fluid depth. They call this the advective regime, which implies that advection of vorticity into the boundary layer becomes important for the heat flux. This mechanism is more effective at free than at rigid boundaries. However, they do not make a comparison with an identical calculation for rigid boundaries. Gough, Spiegel & Toomre (1975), on the other hand, compare very truncated solutions for two rigid and two free boundaries at high Rayleigh number over a wide range of Prandtl numbers. The power laws are identical functions of R_* up to the highest Prandtl numbers, for which $N_* \propto R_*^{\frac{1}{3}}$ for free boundaries and $N_* \propto (R_* \ln R_*)^{\frac{1}{3}}$ for rigid ones.

The second aim of this study was then to determine the constants A and n in an equation equivalent to (5) for high Rayleigh number convection but with heat flux across only an upper free water surface ($N = AR^n$), a somewhat different experimental set-up from the classical one with the fluid enclosed between two parallel plates.

3. Instrumentation and experimental procedure

To simulate approximately a vertically semi-infinite and horizontally infinite layer of water, with heat coming out of the top surface into still air, a tank 0·75 m long, 0·50 m wide and 0·50 m deep was used. The walls of the tank are made of 15 mm thick Plexiglas and insulated by three layers of foam-rubber, each 25 mm thick. The bottom of the tank is made of 25 mm thick Plexiglas and is insulated by a layer of 25 mm thick foam-rubber and a layer of 50 mm thick styrofoam. The water level was usually about 50 mm below the rim of the tank. Tap water was used most of the time. Distilled water was used several times to check the results but no difference was found. The water surface was cleaned by skimming and tissuing off any surface film. Flushing was, however, not possible, since it would disturb the convective motions. However, as noted above, in water with depths > 10 mm the effects of variations in surface tension are predicted to be less important than buoyancy effects (Pearson 1958). This has been verified by Berg & Morig (1969). A compact surface film would have more severe effects on the motion. It is likely that some surfactant materials were present in such a large tank. However, we do not believe that they have affected the results substantially.

The motion in the fluid was visualized using tracers which consisted of a rheoscopic fluid made from fish scales† (Matisse 1974). The tracers are tiny crystals that align themselves with the shear in the flow. To observe the convection pattern on the surface, without interference by scattered light from below, a collimated beam of cool light was used to illuminate just the surface plane. Photographs were taken on Kodak Tri-X film. In order to see the vertical motion, a laser beam passing through a cylindrical lens was used to illuminate a vertical plane. A more sensitive film, Kodak 2475, was used for this photography because the reflected light had very low intensity. (For more details of the photographic technique see Katsaros 1975.)

A Unislide‡ digital-stepping-motor driven assembly provided horizontal as well as vertical movements. The maximum possible horizontal and vertical speeds were 15·5 mm s^{-1} and 21·5 mm s^{-1} respectively while the horizontal and vertical positions

† Manufactured by Kalliroscope Corporation, 145 Main Street, Cambridge, Massachusetts 02142.

‡ Manufactured by Velmex, Inc., P.O. Box 38, E. Bloomfield, New York 14443.

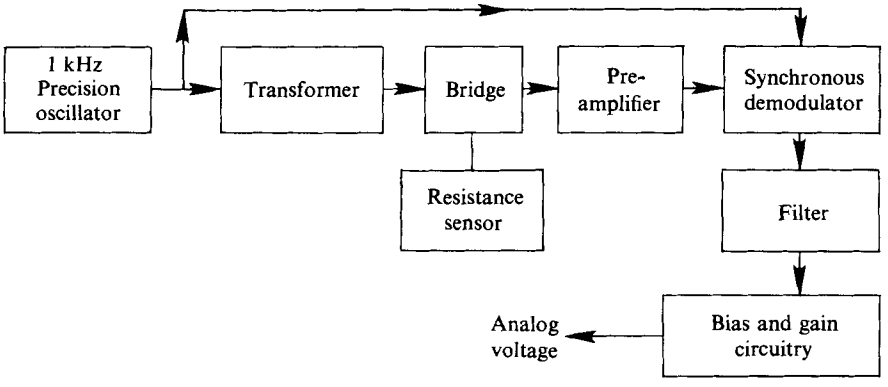

FIGURE 1. Schematic diagram of the resistance-thermometer system.

were accurate to 7·9 and 12·7 μm respectively. The assembly was mounted over the tank with the probe penetrating the surface from above. Mean temperature profiles and profiles of the standard deviation were obtained from about 100 individual profiles collected with 20 mm spacing across the tank. With vertical velocities of 2·5 mm/s, the vertical resolution was 100 μm.

Direct measurements of the temperature distribution within the boundary layer require a sensor with high spatial resolution that minimizes interference with the motion of the fluid. The sensing element consisted of a platinum film vacuum deposited on a Pyrex rod of diameter 15 μm and length 1·2 mm which was overcoated with quartz insulation for operation in conductive solutions. Since temperature changes of 0·01 °C were to be measured (the nominal probe resistance is 6 Ω) and the sensitivity is approximately 0·2 % per °C, the noise level of the system must be less than 0·002 % or it must have a resolution of $1{\cdot}3 \times 10^{-4}\,\Omega$.

The resistance measurements were made with an a.c. synchronous modulation–demodulation resistance-thermometer system (figure 1), a.c. techniques being used to eliminate any spurious thermoelectric noise and drift due to lead junctions, connectors, etc. Synchronous modulation produces an a.c. from a d.c. signal for amplification and the amplified signal was synchronously demodulated to produce a d.c. signal for ease of signal processing. The resistance-thermometer electronics were initially designed for atmospheric temperature measurements using 25 μm platinum wire, where low self-heating, high accuracy and a wide dynamic range were important requirements (Tillman 1972). To minimize self-heating, the total voltage across the sensor was 0·012 V and its temperature variation was approximately $39 \times 10^{-6}\,\mathrm{V\,°C^{-1}}$. Obtaining an accuracy and noise level of 0·01 °C or better with d.c. techniques would require a stability and noise level of 0·39 μV, which is somewhat difficult, since it would require (*a*) that the leads and the resistance-thermometer film be made of identical material, platinum, or (*b*) that all pairs of junctions between dissimilar materials have identical temperatures to within a few hundredths of a degree to minimize the spurious thermoelectric effects. Increasing the power to the sensor would decrease the effect of noise and drift, but would increase the self-heating.

The a.c. source consists of a 1·0 kHz oscillator with frequency and amplitude stability of better than 0·05 % $\mathrm{°C^{-1}}$ and 0·02 % $\mathrm{°C^{-1}}$ respectively. For this application, the pre-amplifier was completely redesigned using transformer coupling to minimize

stray noise pick-up with the probe immersed in conducting solutions in a noisy environment. The amplified signal was subsequently demodulated with full wave rectification, the amplitude of the demodulated signal being a measure of the temperature. A four-pole 25 Hz filter minimizes 60 Hz noise. A bias box follows the demodulator in the present system and is required owing to the limited resolution of the available analog-to-digital converter (0·25 %). Long-term tests of an earlier version of the system have demonstrated a stability equivalent to 0·001 °C for periods of two weeks with a resistor replacing the sensor and the present configuration provides peak-to-peak noise equivalent temperatures of approximately 0·007 °C with a 25 Hz bandwidth.

A temperature profile from the air into the water is continuous across the interface. Thus, in order to determine accurately the position of the surface, an additional probe whose signal changes abruptly when it touches water was mounted in parallel with the temperature sensor. This device, manufactured in our department, employs the change in capacitance which occurs when the tip of a stainless-steel needle becomes surrounded by water. It has a frequency response of at least 50 Hz. The relative vertical separation between the temperature and surface sensor remains constant during data collection. The relative position was, however, determined only to within a millimetre because as one of the sensors makes contact with the water surface, a meniscus creeps up and envelops both.

The data from each vertical profile were collected on magnetic tape. In the analysis the temperature profiles were shifted according to the level relative to the frame of reference (the Unislide track), where the surface sensor turns on. This varied owing to evaporation during the run. The values from each depth were averaged numerically and the standard deviation found. The traverse was adjusted to be parallel to the water surface to within 50 μm, which was tested with the surface sensor. This also ensures that the vertical traverses are perpendicular to the water surface to good accuracy.

The surface level is easily identified in the profiles of the standard deviation of the temperature since the r.m.s. temperature fluctuations are larger by about a factor of two at the first data level above the interface (at a height of 50 μm). A value for ΔT ($= T_b - T_s$) determined from the difference between the average at the top point and the bulk value agrees to within 2 % with the ΔT obtained from the heat flux and equation (19) below. Inaccuracies in the vertical position after averaging and in the heat flux can account for this difference.

Two different methods were used to obtain ΔT in the N *vs.* R study. A Barnes PRT5 infra-red radiometer with a spectral pass band between 8 and 14 μm was used to measure the temperature of the top 50 μm of water. The radiometer looked down vertically from 1·60 m above the water surface. Since it had an angular opening of 2°, it averaged the temperature of a circular area of 56 mm diameter. The radiometer output signal was recorded continuously after passing through a 5 s averaging circuit. The water under the radiometer was stirred at certain intervals to eliminate the boundary layer, and reveal T_b to the radiometer. According to the manufacturer, the radiometer has a sensitivity better than 0·1 °C. The averager eliminated all of the random noise, making it possible to read the temperature change to about 0·06 °C. However, some of the values of ΔT are small and the lack of temperature sensitivity may be an important cause of the scatter in the data.

In a second experiment, which served as a check, ΔT was measured by the resistance film probe. To obtain the surface average, the probe was so adjusted that it barely touched the surface of the water and a horizontal traverse was made. Since it is difficult to locate the surface of the water precisely with the meniscus present, the probe was moved down about 25 μm and another traverse was made. The two averages so determined were again averaged to give T_s. To compensate for any cooling during the period of measurement, a horizontal average was determined at a depth of about 0·15 m before and after the surface runs were made. The two averages at 0·15 m were then averaged to give T_b. $\overline{\Delta T}$ was then determined from the difference.

In both experiments, the heat loss was determined by calorimetry simultaneously with the determination of $\overline{\Delta T}$.

The average heat flux $\bar{Q}$ per unit area of the surface is given by

$$\bar{Q} = \rho c_p d(\partial \overline{T}_b/\partial t) - C, \tag{6}$$

where C is a correction for the heat loss through the walls. $\bar{Q}$ depends on T_a, the air temperature in the laboratory, $\overline{T}_w$, the wet bulb temperature in the laboratory, and on $\overline{T}_s$, which is related to $\overline{T}_b$ by $\overline{T}_b = \overline{T}_s + \overline{\Delta T}$. In the experiments, $\overline{T}_b$ was measured periodically with a mercury-in-glass thermometer to 0·01 °C accuracy. $\bar{Q}$ was then calculated from (6) and plotted against the average bulk temperature for that period. Whenever $\overline{\Delta T}$ was measured, $\overline{T}_b$ was also determined and the corresponding value of $\bar{Q}$ was obtained from the plot.

A separate experiment was performed to determine C. The tank was filled with water until it touched a cover made of the same material as the walls and identically insulated. $\overline{T}_b$ was again recorded as a function of time and the average heat flux per unit area through the side walls, lid and floor of the tank,

$$\bar{Q}_w = \rho c_p [\tfrac{1}{2} lbd(lb + bd + ld)]^{-1} d\overline{T}_b/dt,$$

where l, b and d are the length, breadth and depth of the tank, was determined as a function of $\overline{T}_b - \overline{T}_a$. From this function, the correction

$$C = (2(l+b)\,d/lb + 1)\,\bar{Q}_w \tag{7}$$

can be evaluated for any value of $\overline{T}_b - \overline{T}_a$. Since $\overline{T}_a$ and $\overline{T}_w$ are fairly constant in the laboratory and $\overline{\Delta T}$ is found to be constant during an experiment, C can be determined from $\overline{T}_b$. C was always less than 10 % of $\bar{Q}$.

A data-collection run took approximately 1 to 1½ h. During this time the mean temperature of the tank decreased by about 1 °C depending on the heat flux. It is assumed that the mean profile shape remained approximately constant in spite of the drift. The drift was accounted for in the calculation of the standard deviation in temperature. The scaling length was only weakly changed by the temperature drift, since $\delta \propto Q^{-\frac{1}{4}}$ (e.g. Katsaros & Liu 1974) and Q changed by less than 10 % during a run.

Mean temperature profiles were also obtained by averaging along horizontal traverses through the tank. Any errors in the adjustment for temperature drift affect the mean profile in this case, and the shift in surface level due to evaporation was not measured nor accounted for. There is therefore larger scatter in these data. Otherwise the results of the two techniques are in agreement.

In presenting the data, the deviation of the mean temperature from the bulk value has been scaled with a value for the total $\overline{\Delta T}$ obtained from the heat flux measurement

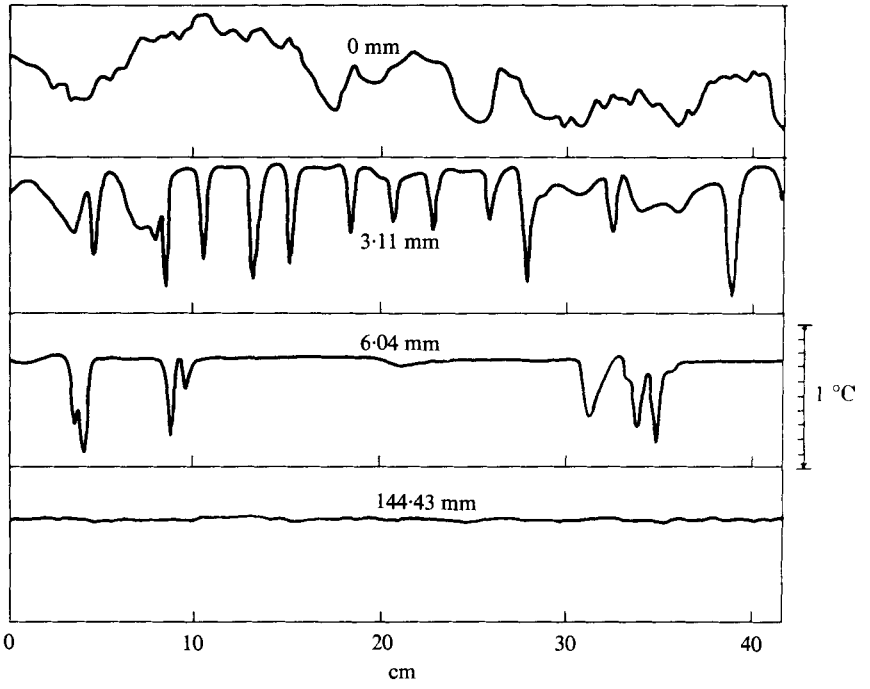

FIGURE 4. Horizontal distribution of temperature at different depths. Bulk water temperature was 31·2 °C. Dry and wet bulb temperatures of the air were 21·6 °C and 12·6 °C respectively.

and the relationship for Nusselt number *vs.* Rayleigh number found in this study, equation (19) below. The depth has been scaled with the δ obtained from the conduction equation.

4. Results and discussion

With the help of the rheoscopic fluid one can observe how the water in the cool surface layer converges along lines and then plunges downward. Viewing from the top, the plunging lines have no definite cellular pattern in turbulent convection. They grow, fade and shift position continuously. Figure 2 (plate 1) is a typical view of the surface at moderate heat flux. The narrow dark lines are regions of sinking motion. A cross-sectional view through a sinking line close to the surface is shown in figure 3 (plate 2). The paths traced out by the crystals reveal the convection pattern near a plunging area. The observations in this experiment agree quite well with those of Spangenberg & Rowland (1961), although the patterns are more chaotic in the present case, probably because the Rayleigh number in this study is larger by two orders of magnitude.

Because of these motions in the boundary layer, the temperature varies with horizontal position and with time. A typical set of records of the variation of temperature in the horizontal at four depths under the same conditions is shown in figure 4. At the surface and in a region within about 0·1 mm under it the temperature variation is disorganized. Since this is the only experiment with measurements so close to the interface, it is not known whether such a region exists near a rigid boundary. Further from the surface, the variation becomes organized into periodic cold deviations from

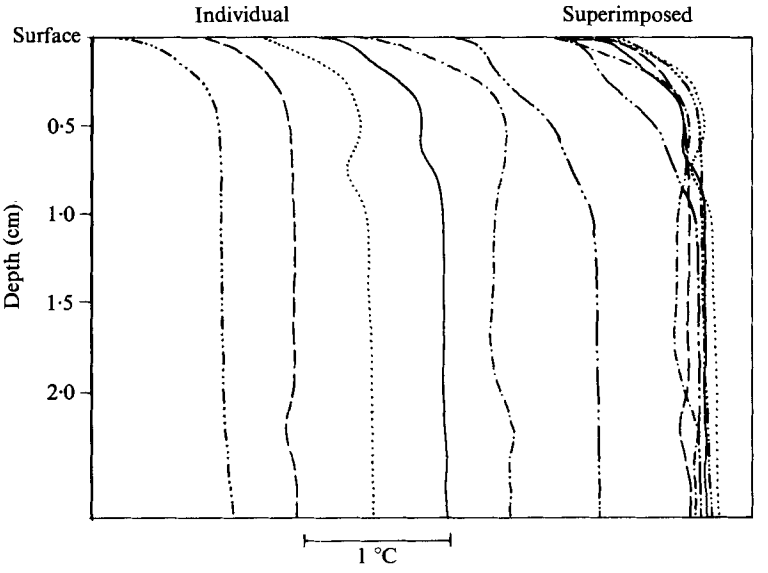

FIGURE 5. Examples of temperature profiles obtained through the thermal boundary layer in 29 °C water. (See text for description of apparatus.) Dry and wet bulb temperatures of the air were 22 °C and 14 °C respectively.

an almost constant temperature. The magnitude of these cold deviations decreases and the average spacing between them increases with increasing distance from the surface. There are no large deviations in the bulk of the fluid. From these data and visualization of the flow, we can deduce that the cold fluctuations are due to cold water plunging down from the boundary layer just under the surface, similar to the columns of hot air observed in laboratory experiments by Townsend (1959) and by Tillman (1972) and others in the free atmosphere. Figure 5 contains several vertical temperature profiles obtained at a constant mean heat flux. Their shapes near the interface are similar to the ones calculated by Foster (1971) for different stages in the cooling cycle of the periodically unstable boundary layer. Thus an intermittent removal of the boundary layer appears to be a valid description of the cause of temperature fluctuations in turbulent free convection. Figure 6 shows the mean temperature profile and its standard deviation for one run.

Our laboratory tank cools in response to the temperature and humidity difference between the water surface and the room. Since any fluctuations in the surface temperature T_s result in a larger fractional change in ΔT than in Q, the boundary condition of constant heat flux applies most closely to the present case. However, the time averaging reduces the difference between the two boundary conditions and the error introduced by the quasi-steady assumption.

Figure 7 shows how well the three theoretical profiles (1), (2) and (3) approximate the experimental data. A comparison between the three theoretical profiles on the one hand and the observations on the other brings out some systematic differences. Lower layers show the effect of the falling cold thermals, which carry a cold deviation to the outer layer compared with conductive cooling, while near the surface the upward advection of warm water appears as a positive deviation.

The effect of the thermals is even more evident when one compares the measured

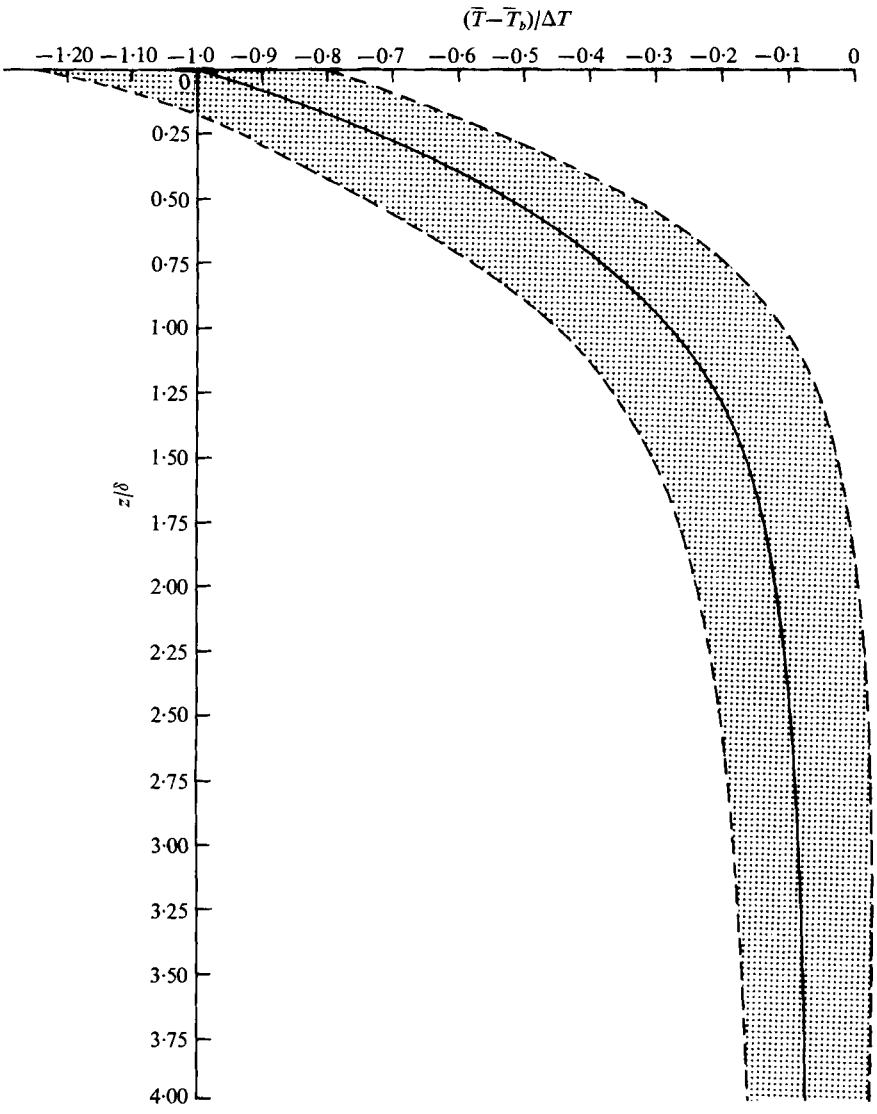

FIGURE 6. Horizontally averaged vertical temperature profile (solid line) and r.m.s. temperature fluctuations (shaded area), obtained from 100 vertical traverses at a heat flux of 210 W m^{-2} and $\Delta z/\delta = 0{\cdot}2$. The shaded area represents one standard deviation of temperature from the mean. The fluctuations are not caused by errors of measurement but *represent* the systematic fluctuations. Note, however, that the temperature distribution is highly skewed (figure 9), the cold deviations being larger in magnitude than the warm ones, so that a deviation of $+\sigma_T$ from the mean is very rare.

profiles of the standard deviation of the temperature with predicted ones (figure 8). The predicted values of the standard deviation σ_T were calculated numerically using the definition

$$\sigma_T^2(z) = \frac{1}{t_*}\int_0^{t_*} [T(z) - \overline{T}(z)]^2\, dt, \tag{8}$$

where t_* is the period of the conductive phase in the life cycle of the thermal boundary layer, where the $\overline{T}(z)$ values are obtained from (1) or (2) and where the corresponding

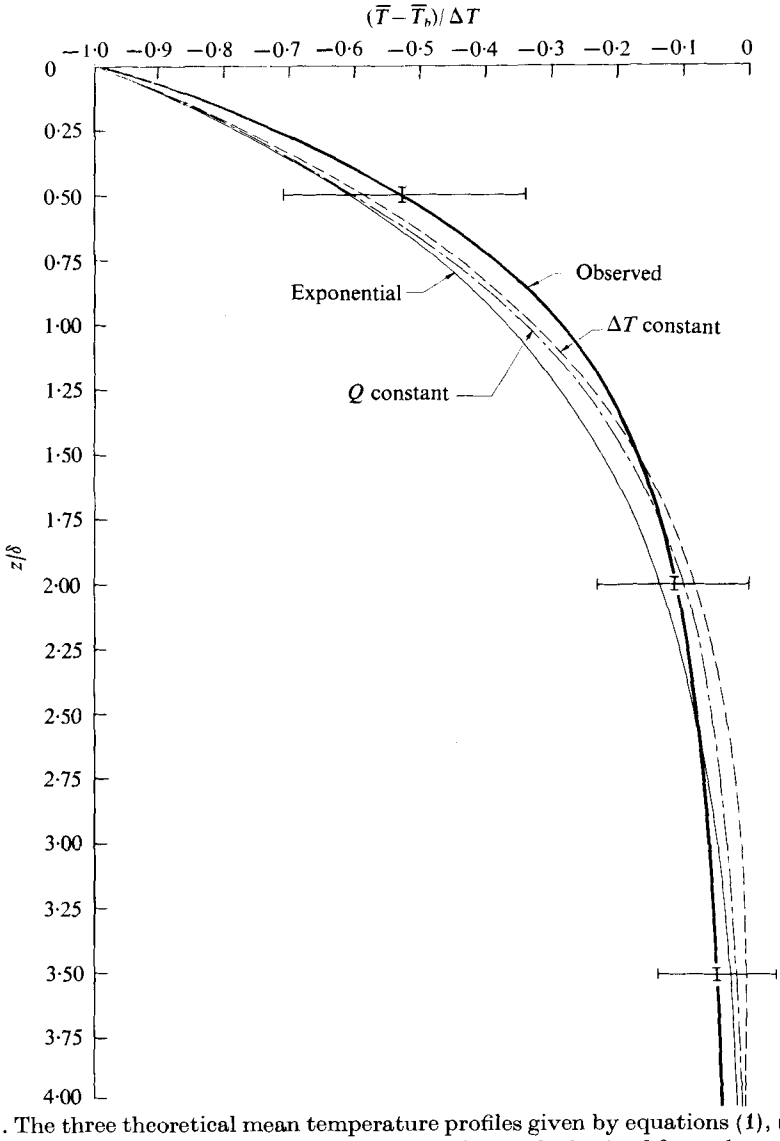

FIGURE 7. The three theoretical mean temperature profiles given by equations (1), (2) and (3) and a mean profile obtained by averaging three mean profiles each obtained from about 100 individual profiles at heat fluxes of 210, 279 and 397 $\mathrm{W\,m^{-2}}$. The bars represent the values of the r.m.s. temperature fluctuations for one run and the vertical resolution respectively.

instantaneous conduction profiles $T(z,t)$ for the two boundary conditions are the familiar ones applicable to a half-space:

$$T(z,t)-T_b = \Delta T \operatorname{erfc}(z/2(\kappa t)^{\frac{1}{2}}) \tag{9}$$

for constant boundary temperature and

$$T(z,t)-T_b = \frac{2Q(\kappa t)^{\frac{1}{2}}}{\kappa\rho c_p} i\operatorname{erfc}\left(\frac{z}{2(\kappa t)^{\frac{1}{2}}}\right) \tag{10}$$

for constant heat flux.

It is interesting to note that the r.m.s. fluctuations near the interface are large and lie between the predicted values for the two extreme boundary conditions, in agreement

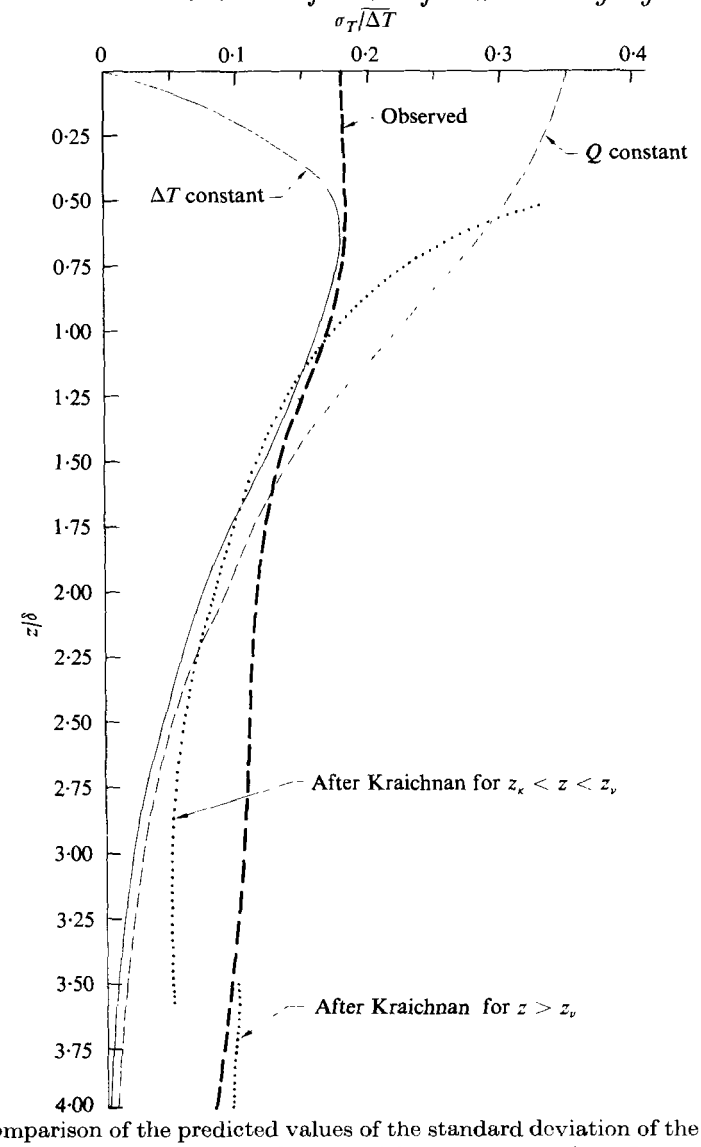

FIGURE 8. Comparison of the predicted values of the standard deviation of the temperature from the conduction equations for the boundary conditions of constant heat flux and constant surface temperature and Howard's assumption of $t_* =$ constant with the average of three sets of data each obtained from about 100 vertical traverses at mean heat fluxes of 210, 279 and 397 W m^{-2}.

with the fact that the boundary condition in the experiment is quasi-steady heat flux and quasi-steady surface temperature. The non-dimensional magnitudes agree with those obtained from laboratory experiments in air by Deardorff & Willis (1967*a*), when consideration has been given to the difference in the scaling temperature ΔT for different boundary conditions.

The distribution of temperature excursions from the mean is highly skewed with large cold excursions being infrequent and very small warm deviations occurring frequently. Since the distribution is non-Gaussian, the shading in figure 5 is only an indication of the r.m.s. fluctuations. One standard deviation was used as a measure but it does not indicate the true extent of warm and cold excursions. In order to obtain

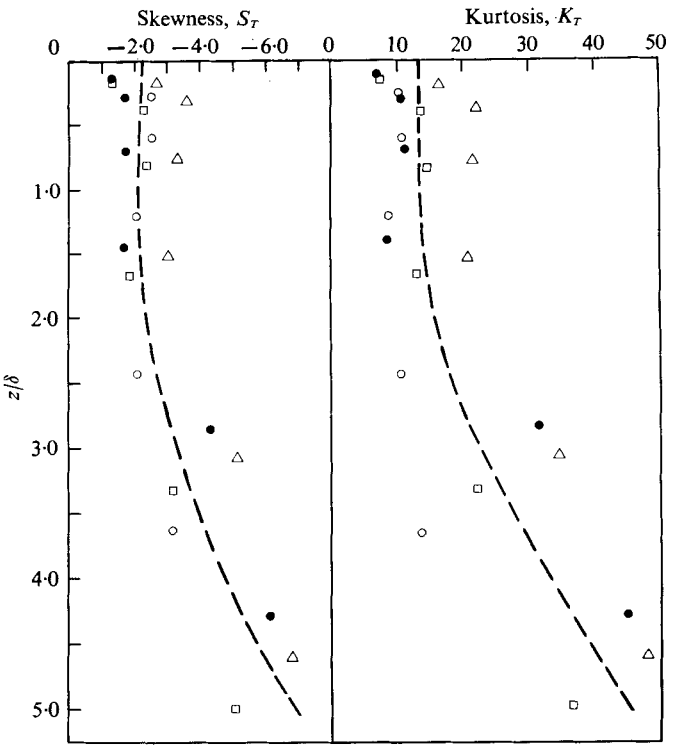

FIGURE 9. Skewness and kurtosis of horizontal temperature traces at several depths obtained by averaging over 20 traverses 0·50 m long at each level. ○, $Q = 179\,\mathrm{W\,m^{-2}}$; ●, $Q = 265\,\mathrm{W\,m^{-2}}$; △, $Q = 370\,\mathrm{W\,m^{-2}}$; □, $Q = 537\,\mathrm{W\,m^{-2}}$.

a measure of the non-Gaussian shape of the distributions, the skewness S_T and kurtosis K_T were calculated from the temperature records obtained during horizontal traverses. The averages from twenty traverses at each depth are given in figure 9, where the depth has been scaled with δ and the following definitions of S_T and K_T were used:

$$S_T = \overline{(T-\bar{T})^3}/\sigma_T^3, \quad K_T = \overline{(T-\bar{T})^4}/\sigma_T^4. \tag{11),(12}$$

The large negative skewness and large kurtosis are typical of highly peaked temperature distributions with a longer tail towards cold deviations. The skewed temperature distribution of this experiment is similar to that observed in the atmospheric surface layer except for a change in sign (Tillman 1972).

The skewness is seen to be fairly constant for $z/\delta < 1$ although the scatter is large, with an almost linear increase (larger negative skewness) at greater depths. This is so because the further away from the boundary that the trace is obtained the more uniform is the environment, and the warm deviations from the mean therefore become very small. The cold deviations also decrease in amplitude with depth but less rapidly.

The kurtosis also increases dramatically with depth because there are fewer and fewer descending plumes (or sheets) that have had enough potential energy to penetrate to such large depths. Those that do reach great depths all have a strong cold deviation from the mean temperature. The warm deviations become very small and almost constant. Thus the temperature distribution becomes more and more lepto-

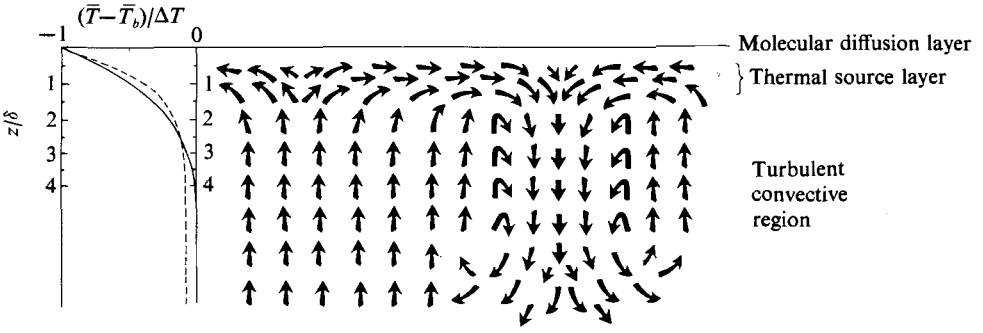

FIGURE 10. Schematic diagram of a model of the thermal boundary layer delineating the source region of the cold thermals. ——, theoretical mean temperature profile based on time-averaged conductive profiles; – – –, mean observed temperature profile. $\bar{T}_b$ = mean bulk temperature, ΔT = total temperature drop, z = vertical co-ordinate, $\delta = k\Delta T/Q$, where k = thermal conductivity, Q = total vertical heat flux.

kurtic. The skewness and kurtosis continue to increase, but more slowly, to a depth of 10δ. Systematic measurements of the temperature fluctuations were not made beyond this depth. However, it is likely that the skewness remains large with increasing depth even though σ_T decreases. When there are two sources of vertical motion, from an upper and a lower surface, interaction takes place in the central region and temporal and horizontal temperature traces appear more symmetric (cf. Deardorff & Willis 1967*a*; Carroll 1971).

It can be seen that δ is the appropriate scaling length for all four of the parameters $\bar{T}$, σ_T, S_T and K_T. In free convection there is only one independent variable, Q, ΔT or δ, since by (4) and (5) two of them can be eliminated.

One can draw further conclusions about the boundary-layer removal from the differences between an observed mean temperature profile and one of the theoretical predictions based on time (or space) averaged molecular conduction profiles [equations (1)–(3)]. Figure 10 is a sketch of the boundary layer where three regions have been identified. The names given to these layers are suggestive of the characteristics of the motion in each layer inferred from the profiles.

Naturally, the assumption that the time t' of the boundary-layer collapse is negligible compared with the time t_* of build-up (or equivalently that the fractional area occupied by falling cold water is infinitely small) must be an approximation. Examining the effect of the finite time and spatial scale of the boundary-layer drainage on the observed profiles can perhaps tell us how thick the layer is from which the cold water stems. Comparing the observed profiles, scaled with δ, with the exponential curve, we note a region at the interface approximately $0{\cdot}1\delta$ in thickness where the observed profiles agree almost exactly with the conduction profile. This layer is so thin that the time constant for adjustment to conductive heat flux is only about 0·5 s. Thus conduction and radiation are the dominant modes of vertical heat transport (McAlister & McLeish 1969). A term used for such a diffusive layer in modelling gas exchange between the sea and the atmosphere is the 'stagnant layer' (e.g. Kanwisher 1963). For gas exchange it has found acceptance because of good agreement between calculated and observed exchange rates. The deduced thickness of the 'stagnant layer' for gas exchange is typically of the order of 100 μm. Because of the short time constant for

such a thin layer, it can not be distinguished whether it takes part in the turbulent exchange or not. We might call this the 'molecular layer'.

Just below this thin surface layer the observed mean profile is warmer than any of the mean conduction profiles. This layer is termed the 'thermal source layer' because it is visualized as the source for the cold water producing the plunging sheets. As this water falls out of the layer, by continuity it is replaced by warmer water from below. The result is net upward warm advection into this region, causing the mean observed profiles to be warmer than the time average of pure conduction profiles would indicate. Even though the boundary-layer collapse model leading to the theoretical profiles [equation (1), (2) or (3)] implies that warm water is moved upwards, the calculated mean profile does not reflect this because it is simply a time average over the instantaneous conduction profiles including profiles both warmer and colder than the mean. This profile can be described as a 'mean non-steady-state conduction profile'.

At the bottom of the 'thermal source layer' there is maximum warm vertical advection, since the replacement water for the whole source layer has to come through that level. Consequently, the level of maximum warm deviation in the profile delineates the bottom of the source layer. This level is not very well defined in figure 7, because of the three possible theoretical ones, but it is located somewhere between $z/\delta = 0{\cdot}5$ and $1{\cdot}0$. Below this thermal source layer there is one level where the downward vertical advection of cold water equals the upward advection of warm water. This is the cross-over point of the observed mean profile with a conduction one. Below this level the cold thermals or falling sheets produce a cold deviation relative to the theoretical profile. At depths where the influence of molecular conduction in the vertical vanishes, the upward advection has little effect on the temperature profile since the $\partial T/\partial z$ of the environment is near zero, but the cold advection continues until horizontal diffusion and entrainment eliminate the temperature contrast. The depths of the layers defined above are 0 to $0{\cdot}1\delta$ for the 'molecular layer' and $0{\cdot}1\delta$ to approximately $0{\cdot}5\delta$ for the 'thermal source layer'. For a heat flux of $210\,\mathrm{W\,m^{-2}}$, the 'molecular layer' would be $250\,\mu$m thick and the 'thermal source layer' would reach to a depth of about 1·25 mm.

To account properly for the effects of horizontal and vertical advection, one would need to solve the complete equation, viz.

$$\partial T/\partial t + \mathbf{V} \cdot \nabla T = \kappa \nabla^2 T. \tag{13}$$

However, the conduction mode of vertical heat transfer certainly appears to dominate the shape of the observed temperature profiles to a depth of 2δ. The addition of vertical-advection considerations adds only a 5–10 % refinement. Nonetheless, these small systematic differences between the observed profiles and predicted 'mean non-steady-state conduction profiles' are instructive.

In a theoretical study of free convection Kraichnan (1962) divided the convective flow into three regions in the case of deep fluids of high Prandtl number (i.e. $P > 0{\cdot}1$). In the one nearest the boundary, $z < z_\kappa$ (the depth where eddy and molecular heat transfer are of equal magnitude), molecular heat conduction and viscosity dominate the flow. In the region $z_\kappa < z < z_\nu$ (the depth where eddy and viscous momentum transfer are of equal magnitude), heat is transferred predominantly by eddy motion while momentum is transferred by molecular viscosity. Beyond z_ν, eddy transfer of

both heat and momentum dominates. By order-of-magnitude arguments he predicted approximate values for z_κ, z_ν, $(\overline{T}-T_b)/(T_s-T_b)$ and σ_T as well as other quantities. z_κ is given by

$$z_\kappa \sim \tfrac{1}{2}\, d/N, \tag{14}$$

which with our definition of δ and $N = d/\delta$ leads to $z_\kappa = \frac{1}{2}\delta$. z_ν is given by $z_\nu \sim 3{\cdot}3P^{\frac{1}{2}}z_\kappa$, which for water gives

$$z_\nu \sim 3{\cdot}6\delta. \tag{15}$$

In our notation

$$\left.\begin{aligned} \sigma_T &\sim 0{\cdot}17\, 2\Delta T(z/z_\kappa)^{-1} \quad \text{for} \quad z_\kappa < z < z_\nu, \\ \sigma_T &\sim 0{\cdot}18P^{-\frac{1}{3}}\, 2\Delta T(z/z_\kappa)^{-\frac{1}{2}}, \quad \text{for} \quad z < z_\nu, \end{aligned}\right\} \quad \frac{\overline{T}-T_b}{T_s-T_b} \sim \sigma_T. \tag{16), (17}$$

σ_T values from (16) and (17) are given by the dotted curves in figure 8, and are seen to be in fair agreement with observations away from the joints z_κ and z_ν.

$$(\overline{T}-T_b)/(T_s-T_b) \sim \sigma_T$$

is only a crude approximation, however.

Carroll (1971), who obtained measurements in air enclosed between rigid boundaries, also found good agreement with Kraichnan's predictions. In particular he found the skewness to have a minimum and σ_T to have a maximum at z_κ. One could possibly interpret our data as showing z_κ to be a level where the skewness begins to increase (i.e. it becomes more negative). The level $z_\kappa = 0{\cdot}5\delta$ does coincide with the maximum of σ_T in our data as well. However, while Carroll's data for σ_T decrease towards the boundary, ours remain almost constant on approaching the free surface. This is probably due to the difference in the thermal boundary conditions. In case of a rigid boundary the surface temperature is held constant while in our case the constant-heat-flux condition is approached.

Our measured profiles do not exhibit the 'knees' seen in some other studies (e.g. Thomas & Townsend 1957; Somerscales & Gazda 1969; Chu & Goldstein 1973; Chang & Wagner 1975), i.e. a region warmer than the water in the central region below the cold upper boundary layer and/or an equivalent cold 'knee' at the lower heated boundary. Herring's (1964) and Veronis' (1966) theories also resulted in mean profiles which had a change in the sign of the temperature gradient just outside the boundary layer. Herring considers this a necessary consequence of his assumption of a non-fluctuating system and the $N \sim R^{\frac{1}{3}}$ power law. The choice of a non-fluctuating system is of course unrealistic. Veronis comments on it as being contrary to his intuition. Neither does Elder (1969), who extended Herring's approach and also obtained a 'bump', although smaller, consider it realistic. Goldstein & Chu (1969), studying convection in air, did not have a change of sign in the slope of their temperature profiles, which in fact are in very good agreement with ours. Deardorff & Willis (1967*a*, *b*) also found a constant sign of the slope of the temperature profiles.

The observed profiles exhibiting a 'knee' were obtained at Rayleigh numbers less than approximately 10^7 in convection between two rigid boundaries except by Chang & Wagner (1975), whose basic aim was wave effects on ΔT. They measured overshoot in their temperature profiles (without waves) below the free water surface in a deep tank, and although their experimental conditions are not spelled out in detail it appears that they had free convection conditions. (They make a comparison with the results of

Spangenberg & Rowland 1961.) Our case, at a Rayleigh number of 10^9 with only one boundary a source of thermals, comes closer to having fully turbulent convection which is independent of the depth than the earlier studies. With two sources of thermals separated by relatively short distances, the warm water released from the lower boundary layer evidently retains some buoyancy and travels across the whole fluid depth, collecting near the cold boundary and producing a region warmer than the bulk or central region. Similarly, cold water collects above the heated lower boundary, producing the colder than bulk 'knee' there. However, in some cases (Thomas & Townsend 1957; Sommerscales & Gazda 1969) the profiles are not symmetric. These cases have been explained as being dependent on circulations caused by the apparatus; see Chu & Goldstein (1973), who themselves found symmetric profiles with gradient reversals. Our lack of overshoot corroborates their suggestion that the upper limit on the Rayleigh number for gradient reversals in water is about 8×10^6. They also indicate that the Rayleigh number where reversals in the temperature profiles end is Prandtl number dependent.

Another indication of depth independence of the convection in these experiments was given by the results of the heat flux *vs.* ΔT measurements. The resulting value for the power n in (5) is very close to $\frac{1}{3}$. However, we should keep in mind that the upper-bound calculations as well as the free-boundary calculation of Moore & Weiss (1973) predict a power greater than $\frac{1}{3}$.

To calculate A and n, 110 pairs of Q *vs.* ΔT data were employed. In 88 pairs the ΔT were found with the radiometer and in 22 pairs with the resistance film probe. A relation of the form of (5) was assumed and a linear regression was found to give

$$\log_{10} NR = -0{\cdot}8059 + 1{\cdot}3311 \log_{10} R \tag{18}$$

with a correlation coefficient of 0·997 and a standard error of 0·000627. (NR is correlated with R in order to separate variations in ΔT from those in Q, as suggested by Globe & Dropkin 1959.) This corresponds to

$$N = 0{\cdot}156 R^{0{\cdot}33}. \tag{19}$$

Figure 11 is a plot of the combined sets of data. It is encouraging to see that there is good overlap of the results obtained by two different methods. These two data sets are tabulated by Liu (1974).

In order to compare the results of this study with previous ones, we have to take into consideration the difference between the definitions of ΔT_* in case of two boundary layers and ΔT when there is heat flux across only one boundary. In the classical two-plate arrangement, the temperature at the boundaries is kept constant and uniform and the temperature difference ΔT_* across the fluid has usually been determined by measuring the temperature difference between the plates. It was shown above that most of the temperature changes in the fluid occur at the boundaries and that the bulk temperature is rather uniform. (The extent to which this statement is true is Prandtl number dependent; e.g. see Kraichnan 1962.) In water the boundary layers are relatively thin and it is therefore reasonable to assume that $\Delta T = \frac{1}{2}\Delta T_*$. Substituting ΔT for ΔT_* in the classical definition of the Nusselt number N_* and Rayleigh number R_* gives the conversion factors needed to compare our results with previous rigid-plate experiments, viz.

$$N = A_* 2^{1+n} R^n. \tag{20}$$

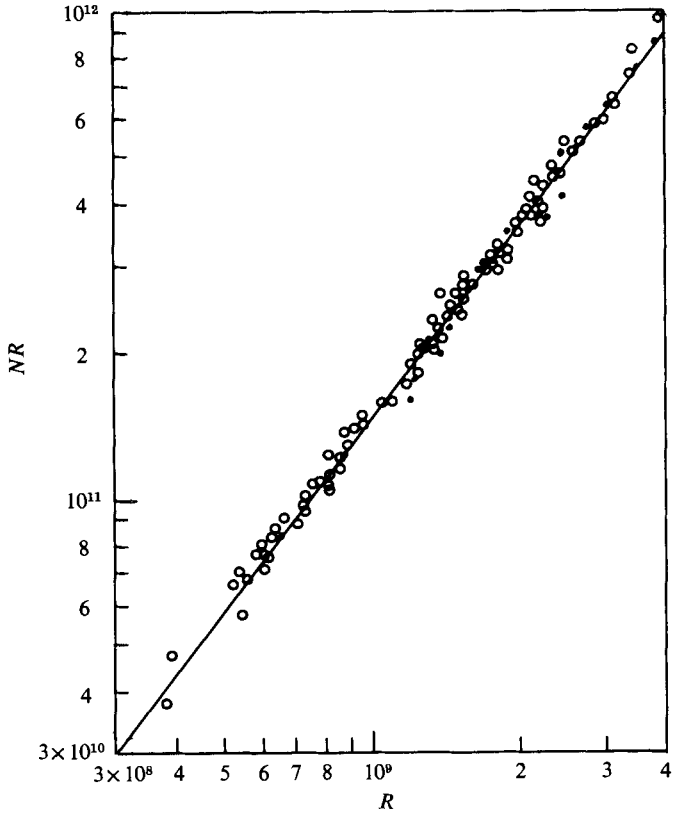

FIGURE 11. The average heat-transport relation for natural convection under a free surface. ——, equation (19); ○, ΔT determined by radiometer; ●, ΔT determined by the resistance film probe.

A warning must be pronounced here. Such a conversion cannot be quite proper unless R is very large, because in a one-sided experiment there is no interaction between thermals from opposite boundary layers, while it has been observed that the flows originating from two rigid boundaries were well correlated at $R_* \simeq 10^7$ (Busse, private communication). Furthermore, in our experiments T_s is not constant, rather Q is quasi-constant, and the velocity boundary conditions differ, but if we assume for the sake of argument that (20) is a valid transformation, then our experiments give

$$N_* = 0{\cdot}062R_*^{0{\cdot}33}. \tag{21}$$

The exponent is not changed by the transformation. It agrees very closely with the value $\frac{1}{3}$ obtained in several theoretical developments but is higher than the values reported in many rigid-boundary experiments. The coefficient is closest to the value obtained by Globe & Dropkin (1959), who also found $n = \frac{1}{3}$. Deardorff & Willis (1967*a*) are in approximate agreement with Globe & Dropkin. Table 1 summarizes the results of previous experiments with water.

One reason for confidence in the validity of the present results is that we have an exceptionally small correction for wall losses, only about 10 %, which has furthermore been measured. The relatively small heat loss through the insulation is due to the large volume-to-area ratio of our tank.

Study	Results	Range of R	N at $R = 10^6$	N at $R = 10^9$
R. J. Schmidt & Saunders (1938)	$N_* = 0{\cdot}098R_*^{0{\cdot}346}$†	3×10^4 to $1{\cdot}5 \times 10^5$	11·67	127·4
Malkus (1954*a*)	$N_* = 0{\cdot}083R_*^{0{\cdot}325}$	5×10^5 to 10^{10}	7·58	71·52
G. Schmidt & Silveston (1959)	$N_* = 0{\cdot}094R_*^{0{\cdot}31}P^{0{\cdot}05}$	$2{\cdot}5 \times 10^4$ to 4×10^5	7·97	67·83
	$N_* = 0{\cdot}11R_*^{0{\cdot}31}$‡			
Globe & Dropkin (1959)	$N_* = 0{\cdot}069R_*^{\frac{1}{3}}P^{0{\cdot}074}$	7×10^6 to 3×10^8	—	—
	$N_* = 0{\cdot}079R_*^{\frac{1}{3}}$‡	—	7·90	79·00
	$N_* = 0{\cdot}76R_*^{0{\cdot}2}$†	—	12·05	47·96
Rossby (1969)	$N_* = 0{\cdot}131R_*^{0{\cdot}30}$	3×10^4 to 3×10^6	8·27	65·66
Chu & Goldstein (1973)	$N_* = 0{\cdot}183R_*^{0{\cdot}278}$	$2{\cdot}8 \times 10^5$ to $1{\cdot}0 \times 10^8$	8·52	58·14
Present work	$N = 0{\cdot}156R^{0{\cdot}33}$	—	—	—
	$N_* = 0{\cdot}062R_*^{0{\cdot}33}$	3×10^8 to 4×10^9	6·00	59·07

† Data reanalysed by Rossby (1969). ‡ Evaluated for $P = 5{\cdot}8$, the value at 27 °C.

TABLE 1. Comparison of the Nusselt numbers in different ranges of Rayleigh number from several experiments.

A more physical method of comparison with other experiments is to look at the values of N_*. However, the maximum R_*'s in our experiments are about two orders of magnitude larger than in other studies. Only if we assume that the experimental results can be extrapolated within the turbulent regime can we make comparisons. Columns 4 and 5 of table 1 are the values of N_* for $R_* \simeq 10^6$ and $R_* = 10^9$ as evaluated from the respective regressions. These two Rayleigh numbers are comparable to the values in past and present experiments. There is obviously large scatter. The N_*'s derived from (21) for those two R_* values are 6·00 and 59·07, respectively, close to the values obtained from the results of the most recent experiments. Figure 12 shows that, within the proper range of Rayleigh numbers, the N_* obtained from this study falls between those from the results of Rossby (1969) and Chu & Goldstein (1973) but our slope is steeper.

Theoretical predictions for the relation between N and R can also be obtained by looking at the boundary layer. If we define a boundary-layer thickness, as Howard (1966) did, we shall have

$$N = Q(k\Delta T/d)^{-1} = d/\delta_H = d/2\delta = (R/R_{\delta_H})^{\frac{1}{3}}, \tag{22}$$

where $R_{\delta_H} = \alpha g \Delta T \delta_H^3/\kappa\nu$ can be interpreted as the Rayleigh number of the boundary layer (Howard's δ_H is twice our δ because his Q is calculated across a fluid with two boundary layers). According to Howard's (1966) theory, $R_{*\delta_H} \simeq R_{*c}$, the critical Rayleigh number. For two rigid boundaries, $R_{*c} \simeq 10^3$, which gives $N = 0{\cdot}252R^{\frac{1}{3}}$ or $N_* = 0{\cdot}1R_*^{\frac{1}{3}}$. For free boundaries the coefficients increase by 16 %, the power remaining constant if one simply inserts R_{*c} for free boundaries. Herring's (1963, 1964) numerical calculations for large R_* also result in a $R_*^{\frac{1}{3}}$ power law and result in an increase in the coefficient by a factor of 2·3 for free boundaries. Kraichnan (1962) suggested that δ is independent of d, on the basis of a mixing-length model, but is related to a transition Péclet number $Pe = w(\delta)\,\delta/k$, where $w(\delta)$ is the r.m.s. vertical velocity fluctuation at $z = \delta$. From his estimation of the Péclet number, it can be deduced that $N = 0{\cdot}224R^{\frac{1}{3}}$

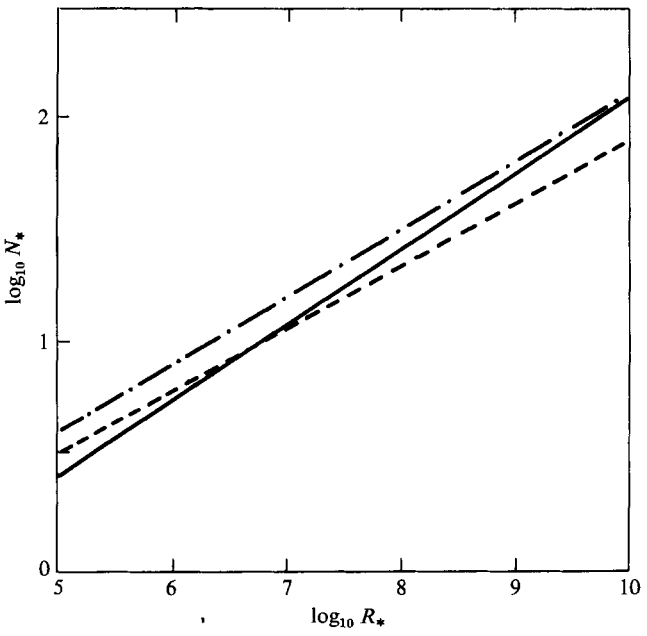

FIGURE 12. A comparison of N_* *vs.* R_* from three experiments. ——, present work; – – –, Chu & Goldstein (1973); –·–·–, Rossby (1969).

or $N_* = 0{\cdot}89R_*^{\frac{1}{3}}$ in high Prandtl number fluid enclosed within rigid boundaries. The disagreement between these predictions and (19) and (21) is not great.

There appears to be much theoretical justification for the $\frac{1}{3}$ power law. However, the recent calculations by Moore & Weiss (1973) predict a power n of 0·365 for water and free boundaries at $R_* = O(10^7)$, which does not agree with our results. Gough *et al.* (1975) obtain a much lower power $[(N(R_* \ln R_*)^{\frac{1}{3}}]$ for Prandtl numbers in the range of water. They do, however, obtain $N \propto R_*^{\frac{1}{3}}$ for high Prandtl and Rayleigh numbers and free boundaries, the power law in this case being lower for rigid boundaries.

Rossby (1969) indicated concern about the accuracy of the physical constants used by different experimenters in the evaluation of N_* and R_*. He noticed differences of 2 % in the values of $k/\rho c_p$ and 2·5 % in α for water at the same temperature, and contributed some of the scatter in the results to this inaccuracy. The values of the physical constants of water used in this study were obtained from *CRC Handbook of Chemistry and Physics*, 52nd edn (1971–72, Chemical Rubber Company). $\bar{T}_b$ in our experiments ranges from 21·6 °C to 42·7 °C. For this range of temperature, c_p and ρ are practically constant. The values $c_p = 4{\cdot}2 \times 10^{-3}\,\mathrm{J\,kg^{-1}}$ and $\rho = 10^3\,\mathrm{kg\,m^{-3}}$ were used for all data, giving a maximum error of 0·2–0·5 % respectively. The variation of k with temperature was also neglected: $k = 6{\cdot}13 \times 10^{-2}\,\mathrm{Wm^{-1}\,°C^{-1}}$ was used, giving a maximum error of 3 %. The values of α/ν, on the other hand, vary strongly with temperature, and were interpolated at 0·1 °C intervals. There is a maximum variation of 6 % for a 1 °C change in temperature. Therefore the values of α/ν will introduce considerable error in the value of R if the temperature of the fluid is not known to an accuracy of better than 1 °C.

In most of the experiments, including this one, the effect of the variation of Prandtl number with temperature on the results is neglected. However, even the maximum

deviation of 25 % from the Prandtl number at the mean temperature of our range only causes a 1·5 % change in A according to the Prandtl number dependence suggested by Globe & Dropkin (1959). The power n would be unaffected.

The comparison between experiments listed in table 1 may not be proper because the experiments covered different ranges of R_*. Both Malkus (1954*a*) and Rossby (1969) observed delicate changes in the heat flux slope within their respective ranges of Rayleigh number shown in table 1. No variations in the slope of NR *vs.* R were seen in the 10^8–10^9 range of R of this study. Neither did Fitzjarrald (1976) find any for air in this range of Rayleigh numbers.

5. Summary

We have in this study looked closely at the temperature structure within the boundary layer below a free water surface, and at the heat transport in a deep layer of water bounded on top by a free surface.

Our tank was too small for examining the horizontal large-scale flow. However, within the boundary layer the motions are probably well represented by the present experimental set-up. Visualization of the flow near the interface showed that the cooled boundary layer plunges down in sheets from narrow lines at the surface and that the spacing between the lines decreases with increasing heat flux. It can be seen in vertical cross-sections that motions persist very close to the interface.

The measured mean temperature profile in the boundary layer of water in turbulent free convection was seen to be highly nonlinear, consistent with the unsteadiness of this layer. Comparison of the mean profiles with theoretical ones based on time averages of the instantaneous conduction profiles show fairly close agreement. The theoretical profiles are based on the assumption that the cooled boundary layer collapses and sinks at a time t_* or at various times randomly distributed between 0 and t_*. These two assumptions span the possibilities for the age distributions. There are some small but systematic differences between the theoretical profiles and the measured mean profile that are due to the assumption that the time of collapse is infinitely small compared with t_*. Actually, what is observed, of course, is that a fraction of the surface has sinking motion below it *at all times* and a larger area has slower upwelling motion.

From the systematic differences between the theoretical conduction profiles and the observed mean temperature profiles one can delineate regions of warm upward advection and cold downward advection. The layer above the maximum vertical warm advection can then be identified as a region providing the cold water for the thermals. It has therefore been termed the 'source layer' and on the non-dimensionalized depth scale reaches to about $z/\delta = 0{\cdot}5$. This is the depth in Kraichnan's (1962) theory where eddy and conductive heat fluxes are of equal magnitude.

The r.m.s. temperature fluctuations agree closely with theoretical predictions based on the boundary-layer collapse theory of Howard (1966) and also with Kraichnan's (1962) predictions between $z/\delta = 0{\cdot}5$ and $z/\delta = 3{\cdot}5$. Near the surface the r.m.s. fluctuations lie half-way between predictions based on Howard's boundary-layer collapse theory for constant ΔT and for constant Q.

The skewness and kurtosis values are consistent with narrow plume-like structures. With the thermals originating at only one boundary, the fluctuations, which diminish in amplitude with depth, become more and more skewed, and do not have a more

random distribution in the centre as seen in two-plate convection experiments (e.g. Deardorff & Willis 1967*a*; Carroll 1971).

The change in the sign of the temperature gradient just below the boundary layer found in some previous experiments was not observed by us. This is explained as being due to a closer approach to complete depth independence, (i) because the Rayleigh number is larger than in most earlier studies, $O(10^9)$, and (ii) because heat flux occurs across only one boundary.

The N *vs.* R relationship showed the Nusselt number to have an almost exact $R^{\frac{1}{3}}$ dependency. We think that this is an accurate result because our heat losses through the walls were small, and could be measured and accounted for. The power may be influenced by the fact that our tank is too small to allow the existence of the horizontal scales several times the depth which are observed in bigger tanks (Deardorff & Willis 1967*a*; Carroll 1971; Fitzjarrald 1976). Kraichnan (1962) shows that the shear instabilities created by the large eddies at the fluid boundaries result in a larger power of R rather than a smaller one. Moore & Weiss (1973) give the same explanation for a power of 0·365 obtained for convection in water between free boundaries. A similar argument has been presented by Businger (1973) for the atmospheric boundary layer when it approaches free convection, which is in agreement with the observed temperature profiles.

The chief limitation of this work lies in the limited size of the convection tank. In view of recent experiments with mechanically produced turbulence in the water, it is felt, however, that the elimination of the larger scales possible in nature for the same Rayleigh number does not appreciably affect the boundary-layer structure.

We are grateful to many individuals who contributed to the establishment of the research facility: Mr H. Lahore contributed to the improved design of the temperature bridge system and built the probe motion controls; Mr Mike Brengle developed the computer routines for probe motion and sampling and assisted with the data analysis; Mr Arnold Weikert manufactured the tank and probe mounts; Mr F. Weller, Mr R. Sunderland and Mr.R. Greyell designed and built the surface sensor. We are especially grateful to Prof. F. H. Busse, who carefully read the manuscript and suggested several improvements. Primary financial support was provided by the Office of Naval Research Contract N00014-67-A-0103-0014 Project no 083–012. Additional support from the U.S. Army Research Grant DAHCO4-74-G-0022 and NSF Grant ATM76-00855 is acknowledged.

REFERENCES

Ball, F. K. 1954 *Austr. J. Phys.* **7**, 649.

Bénard, H. 1901 *Ann. Chim. Phys.* **11**, 1261.

Berg, J. C., Acrivos, A. & Boudart, M. 1966 *Adv. Chem. Engng* **6**, 61.

Berg, J. C. & Mong, C. R. 1969 Density effect in interfacial convection. *Chem. Engng Sci.* **24**, 937–946.

Businger, J. A. 1973 *Boundary-Layer Met.* **4**, 323.

Busse, F. H. 1969 *J. Fluid Mech.* **37**, 457.

Carroll, J. J. 1971 The structure of turbulent convection. Ph.D. thesis, Dept. of Meteorology, University of California, Los Angeles.

Chandrasekhar, S. 1961 *Hydrodynamic and Hydromagnetic Stability.* Oxford: Clarendon Press.

Chang, J. H. & Wagner, R. N. 1975 *J. Geophys. Res.* **80**, 2677.

CHU, T. Y. & GOLDSTEIN, R. J. 1973 *J. Fluid Mech.* **60**, 141.
DANCKWERTS, P. V. 1951 *Ind. Engng Chem.* **43**, 1460.
DEARDORFF, J. W. & WILLIS, G. E. 1967*a* *J. Fluid Mech.* **28**, 675.
DEARDORFF, J. W. & WILLIS, G. E. 1967*b* *Quart. J. Roy. Met. Soc.* **93**, 166.
ELDER, J. W. 1969 *J. Fluid Mech.* **35**, 417.
EWING, G. & MCALISTER, E. D. 1960 *Science* **13**, 1374.
FITZJARRALD, D. E. 1976 *J. Fluid Mech.* **73**, 693.
FOSTER, T. D. 1965 *Phys. Fluids* **8**, 1770.
FOSTER, T. D. 1971 *Geophys. Fluid Dyn.* **2**, 201.
GLOBE, S. & DROPKIN, D. 1959 *J. Heat Transfer* **81**, 24.
GOLDSTEIN, R. J. & CHU, T. Y. 1969 *Prog. Heat Mass Transfer* **2**, 55.
GOUGH, D. O., SPIEGEL, E. A. & TOOMRE, J. 1975 *J. Fluid Mech.* **68**, 695.
HASSE, L. 1963 *Tellus* **15**, 363.
HÄUSSLER, W. 1956 *Wiss. Z. Tech. Hochschule Dresden* **5**, 435.
HERRING, J. R. 1963 *J. Atmos. Sci.* **20**, 325.
HERRING, J. R. 1964 *J. Atmos. Sci.* **21**, 277.
HIGBIE, R. 1935 *Trans. A.I.Ch.E.* **31**, 365.
HOWARD, L. N. 1963 *J. Fluid Mech.* **17**, 405.
HOWARD, L. N. 1966 *Proc. 11th Int. Cong. Appl. Mech., Munich*, 1964 (ed.H. Görtler), p. 1109.
JEFFREYS, H. 1926 *Phil. Mag.* **2**, 833.
JEFFREYS, H. 1928 *Proc. Roy. Soc.* **118**, 195.
KANWISCHER, J. 1963 *Deep-Sea Res.* **10**, 195.
KATSAROS, K. B. 1973 *J. Phys. Ocean.* **3**, 482.
KATSAROS, K. B. 1975 Turbulent free convection in fresh and salt water, some characteristics revealed by visualization. *Rep. Dept. Atmos. Sci., Univ. Wash.*
KATSAROS, K. B. & BUSINGER, J. A. 1973 *J. Geophys. Res.* **78**, 1964.
KATSAROS, K. B. & LIU, W. T. 1974 *J. Phys. Ocean.* **4**, 654.
KRAICHNAN, R. H. 1962 *Phys. Fluids* **5**, 1374.
KRISHNAMURTI, R. 1970 *J. Fluid Mech.* **42**, 309.
KRISHNAMURTI, R. 1973 *J. Fluid Mech.* **60**, 285.
LIU, W. T. 1974 Thermal structure and heat transport in the molecular boundary layer under an evaporating surface of a deep tank of water. M.S. thesis, Dept. of Atmospheric Sciences, University of Washington, Seattle.
LIU, W. T. & BUSINGER, J. A. 1975 *Geophys. Res. Lett.* **2**, 403.
LOW, A. R. 1929 *Proc. Roy. Soc.* A **125**, 190.
MCALISTER, E. D. 1964 *Appl. Opt.* **3**, 609.
MCALISTER, E. D. 1967 *Ocean Ind.* **215**, 35.
MCALISTER, E. D. 1969 *Ocean from Space.* Gulf Publishing Co.
MCALISTER, E. D. & MCLEISH, W. 1969 *J. Geophys. Res.* **74**, 3408.
MCALISTER, E. D. & MCLEISH, W. 1970 *Appl. Opt.* **9**, 2697.
MCALISTER, E. D., MCLEISH, W. & CORDUAN, A. 1971 *J. Geophys. Res.* **76**, 4172.
MALKUS, W. V. R. 1954*a* *Proc. Roy. Soc.* A **225**, 185.
MALKUS, W. V. R. 1954*b* *Proc. Roy. Soc.* A **225**, 196.
MATISSE. P. 1974 A flow-indicating fluid. *Rep. Kalliroscope Corp.*, 145 *Main Street, Cambridge, Mass.*
MOORE, D. R. & WEISS, N. O. 1973 *J. Fluid Mech.* **58**, 289.
MULL, W. & REIHER, H. 1930 *Beihefte Gesundheitsing Ing.* ser. 1, p. 28.
PEARSON, J. R. A. 1958 *J. Fluid Mech.* **4**, 489.
PELLEW, A. & SOUTHWELL, R. V. 1940 *Proc. Roy. Soc.* A **176**, 312.
RAMDAS, L. E. & RAMAN, P. K. 1946 *Indian Acad. Sci. Proc.* A **23**, 127.
RAYLEIGH, LORD 1916 *Phil. Mag.* **32**, 529.

ROLL, H. I. 1965 *Physics of the Marine Atmosphere*. Academic Press.
ROSSBY, H. T. 1969 *J. Fluid Mech.* **36**, 309.
SCHMIDT, G. & SILVESTON, P. L. 1959 *Chem. Engng Prog. Symp. Ser.* **29**, 55.
SCHMIDT, R. J. & MILVERTON, S. W. 1935 *Proc. Roy. Soc.* A **152**, 586.
SCHMIDT, R. J. & SAUNDERS, O. A. 1938 *Proc. Roy. Soc.* A **165**, 216.
SOMERSCALES, E. F. C. & GAZDA, I. W. 1969 *J. Heat Mass Transfer* **12**, 1491.
SPANGENBERG, W. G. & ROWLAND, W. R. 1961 *Phys. Fluids* **4**, 743.
SPARROW, E. M., HUSAR, R. B. & GOLDSTEIN, R. J. 1970 *J. Fluid Mech.* **41**, 793.
STRAUS, J. M. 1973 *Geophys. Fluid Dyn.* **5**, 261.
STRAUS, J. M. 1976 *Dyn. Atmos. Oceans* **1**, 77.
THOMAS, D. B. & TOWNSEND, A. A. 1957 *J. Fluid Mech.* **2**, 473.
TILLMAN, J. E. 1972 *J. Appl. Met.* **11**, 783.
TOWNSEND, A. A. 1959 *J. Fluid Mech.* **5**, 209.
VERONIS, G. 1966 *J. Fluid Mech.* **26**, 49.
WILLIS, G. E. & DEARDORFF, J. W. 1965 *Phys. Fluids* **8**, 2225.
WILLIS, G. E. & DEARDORFF, J. W. 1967*a* *Phys. Fluids* **10**, 931.
WILLIS, G. E. & DEARDORFF, J. W. 1967*b* *Phys. Fluids* **10**, 1861.
WOODCOCK, A. H. 1941 *J. Mar. Res.* **4**, 153.
WOODCOCK, A. H. & STOMMEL, H. 1947 *J. Met.* **4**, 102.

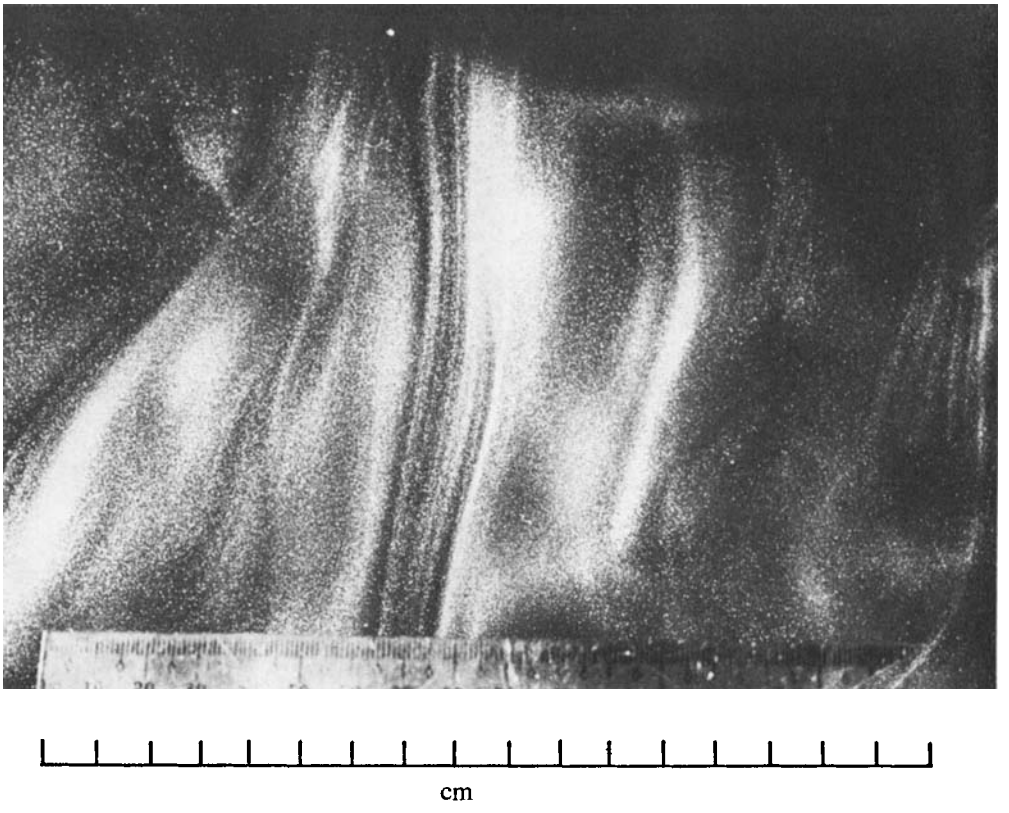

FIGURE 2. Photograph of the horizontal convection pattern just under the free surface of water in free convection. Bulk water temperature was 32·0 °C, dry and wet bulb temperatures of the air were 21·7 °C and 11·6 °C, respectively, and total heat flux was 360 W m^{-2}. Projector lighting, 0·5 s exposure.

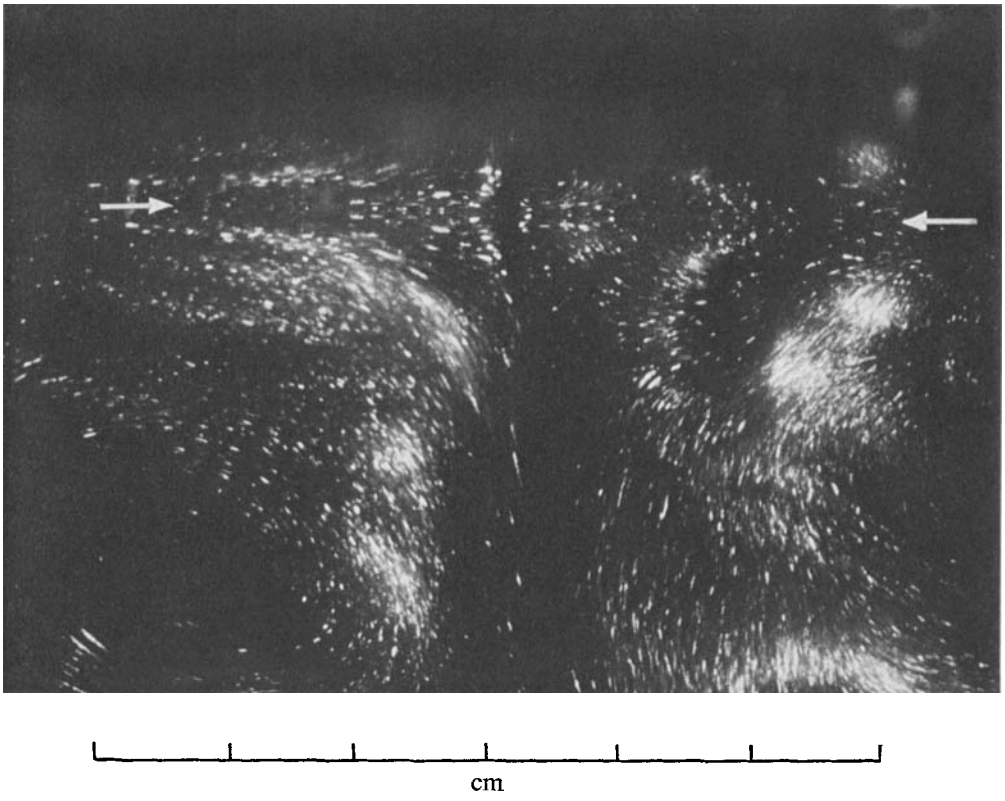

FIGURE 3. Photograph of the vertical convection pattern through a plunging sheet. The interface is seen as the line of reflexion indicated by the white arrows. Bulk water temperature was 33·2 °C, dry and wet bulb temperatures of the air were 23·0 °C and 18·0 °C, respectively, and total heat flux was 270 W m^{-2}. Laser lighting, 3 s exposure.